Available online at www.sciencedirect.com
ScienceDirect
Acta Materialia 56 (2008) 500–510
Acta MATERIALIA
www.elsevier.com/locate/actamat

Effects of free volume changes and residual stresses on the fatigue and fracture behavior of a Zr–Ti–Ni–Cu–Be bulk metallic glass

M.E. Launey [a,1], R. Busch [b], J.J. Kruzic [a,*]

[a] Materials Science, School of Mechanical, Industrial, and Manufacturing Engineering, Oregon State University, 204 Rogers Hall, Corvallis, OR 97331, USA
[b] Universität des Saarlandes, Lehrstuhl für Metallische Werkstoffe, 66041 Saarbrücken, Germany

Received 6 September 2007; accepted 4 October 2007

Abstract

The roles of free volume and residual stress in affecting the fracture and fatigue behavior of a $Zr_{44}Ti_{11}Ni_{10}Cu_{10}Be_{25}$ bulk metallic glass are examined. Different residual stress and free volume states were achieved by annealing below the glass transition temperature. When residual stresses from casting were relieved by annealing, there was an associated decrease in both the fracture toughness and fatigue threshold. Longer and higher temperature annealing resulted in free volume reductions due to structural relaxation that were quantified by enthalpy recovery measurements. Structural relaxation shows a pronounced effect in reducing the fracture toughness and improving the fatigue limit by affecting fatigue crack initiation. However, free volume reduction did not show any influence on the fatigue crack-growth rates or thresholds. This latter effect is attributed to the fact that the large strains at the fatigue crack tip cause a local increase in free volume that appears to dominate the local flow properties, making the initial free volume state irrelevant. The increased free volume associated with this fatigue transformation zone was verified by depth-profiled positron annihilation spectroscopy conducted on the fatigue fracture surfaces. Finally, controlling free volume and residual stresses appears to be a viable way to tailor the fracture and fatigue properties of bulk metallic glasses for given applications.

Keywords: Bulk metallic glasses; Free volume; Fatigue; Fracture; Residual stresses

1. Introduction

Bulk metallic glasses (BMGs) have many attractive properties for structural applications, including high specific and near theoretical strength combined with reasonably high fracture toughness, good corrosion resistance, low damping, large elastic strain limits, and the ability to precisely net-shape into complex geometries [1,2]. One property which has been perceived as a limitation for these materials has been poor fatigue resistance relative to traditional crystalline metallic materials [3,4]; however, not all studies to date have been in agreement on this point, e.g. see Refs. [5–8]. For the most-studied BMG known as Vitreloy 1™ ($Zr_{41.25}Ti_{13.75}Ni_{10}Cu_{12.5}Be_{22.5}$),[2] reported 10^7 cycle fatigue strengths vary by a factor of seven [3,7,9], and fatigue thresholds by a factor of three [3], with the latter variation within a single study. While some of the reported scatter may be explained by different testing configurations [10], this does not account for all the observed variations, e.g., those in [3,9]. It should be noted, however, that potential effects on the fatigue behavior due to residual stresses or free volume variations have been ignored in most fatigue studies on BMGs [3–8].

Residual compressive stresses up to several hundred MPa can form on the surface of BMGs during the casting process [11,12]. Such residual stresses will superimpose on any applied stresses, potentially affecting the fracture and fatigue behavior. Additionally, the free volume is known to be an important factor in determining the mechanical

* Corresponding author. Tel.: +1 541 737 7027; fax: +1 541 737 2600.
E-mail address: jamie.kruzic@oregonstate.edu (J.J. Kruzic).
[1] Present address: Materials Sciences Division, Lawrence Berkeley National Laboratory, Berkeley, CA 94720, USA.

[2] All compositions are given in terms of at.%.

1359-6454/$30.00
doi:10.1016/j.actamat.2007.10.007

properties of BMGs [13–20], a point which has only recently been considered when comparing the fatigue behavior of as-cast amorphous alloys in the absence of hydrogen embrittlement [9]. The deformation of metallic glasses requires the existence of free volume, i.e., extra volume relative to a fully dense glass that is frozen into the atomic structure and allows physical space for atomic movement under mechanical loading [13–15]. Since free volume is needed to allow metallic glasses to deform, a reduction in free volume hinders plastic deformation [13–15]. This reduced flow ability results in lower fracture toughness [9,17–20] and longer fatigue lives [9]. The latter result implies that either the fatigue crack initiation or growth portions of the fatigue lifetime (or both) must increase as free volume decreases. Accordingly, this paper investigates the effects of residual stresses and free volume variations on the fracture and fatigue behavior of a $Zr_{44}Ti_{11}Ni_{10}Cu_{10}Be_{25}$ bulk metallic glass, with specific attention paid to separating the effects on fatigue crack initiation and growth and, when possible, understanding the specific mechanisms involved.

2. Free volume and structural relaxation

Free volume differences may exist in nominally identical metallic glasses in the as-processed state due to differences in their processing conditions. Slower cooling rates result in less free volume [21], and such differences have been detected using differential scanning calorimetry (DSC) and positron annihilation spectroscopy (PAS) measurements [9,21]. Additionally, a reduction in free volume can be achieved via structural relaxation by annealing at a temperature below the glass transition temperature [22,23]. It has been shown that annealing below T_g results in a loss of ductility of conventional metallic glasses [24] and several mechanisms have been proposed, including the formation of a brittle phase, phase separation, or overall densification [16,25].

Characterization of free volume variations is paramount if one wants to understand mechanical properties of metallic glasses such as fracture and fatigue. With PAS it is possible to gain insight into changes in the size and/or concentration of open volume regions, for example those associated with plastic deformation [26–29]. Although, PAS provides information about the distribution of free volume at the nano-scale, it is currently not possible to make quantitative measurements. Conversely, DSC has been used to characterize free volume changes in metallic glasses after structural relaxation, with several efforts focused on quantifying free volume differences [30–35].

3. Experimental methods

3.1. Materials and sample preparation

Experiments were performed on as-cast plates (2.3 mm thick, 85.0×40.0 mm) of fully amorphous $Zr_{44}Ti_{11}Ni_{10}Cu_{10}Be_{25}$, produced and supplied by Liquidmetal© Technologies (Lake Forest, CA). This BMG was chosen because it does not demonstrate phase separation in the supercooled liquid state [36], thus allowing sub-T_g annealing without risk of phase separation and reduced risk of nanocrystallization. Compact tension, C(T), and bend beam specimens were machined from the plates before any subsequent annealing.

Annealing temperature and times were carefully chosen based on the time–temperature–transformation (TTT) diagram for $Zr_{44}Ti_{11}Ni_{10}Cu_{10}Be_{25}$ [37] so that no crystallization would occur. For isothermal structural relaxation, annealing times were integral numbers of the relaxation time, τ. The magnitude of structural relaxation can be calorimetrically observed in the temperature interval, ΔT_g, which is defined as the temperature range between the onset and the end of the endothermic glass transition event. For a constant heating rate DSC experiment, τ can be described as

$$\tau = \Delta T_g / R, \tag{1}$$

where R is the heating rate. The onset value of T_g at each heating rate is the temperature that corresponds to each τ value in the Vogel–Fulcher–Tamman (VFT) relation

$$\tau = \tau_0 \cdot \exp\left(\frac{D^* \cdot T_0}{T - T_0}\right), \tag{2}$$

where D^* is the fragility parameter and T_0 is the VFT temperature, defined as the temperature at which $\tau \to \infty$. τ_0 is the value of the relaxation time in the limit as $1/T \to 0$ and is very similar for all Zr-based bulk metallic glasses, $\sim 2.5 \times 10^{-13}$ s [38]. D^* and T_0 were found to be 31.6 and 321 K, respectively [35]. An annealing temperature of 610 K was chosen because of the reasonable relaxation time at this temperature (at 610 K, $\tau = 438$ s), and isothermal relaxation experiments were done for 1τ and 10τ with the temperature carefully monitored using a calibrated thermocouple placed on the samples. For 10τ, the samples were assumed to be essentially fully relaxed and in a state close to the metastable equilibrium of the supercooled liquid when observed on a long time scale [22].

For some specimens, a stress-relieving anneal was performed at 573 K for 2 min. The purpose of this heat-treatment was to relieve residual compressive stresses at the surface due to thermal tempering during processing. At 573 K, the structural relaxation time is long enough ($\tau \sim 21$ h) so the material did not have time to relax. After annealing, enthalpy recovery experiments [35] were performed for all specimens in a differential scanning calorimeter (DSC) at heating rate of $0.1\ \mathrm{K\ s^{-1}}$ in argon atmosphere (Perkin–Elmer Diamond DSC). The specimens were confirmed to be fully amorphous by high-resolution transmission electron microscopy [35].

3.2. Fracture toughness and fatigue crack growth rate measurements

Fracture toughness and fatigue crack growth experiments were performed on as-received, stress-relieved

(SR), 1τ and 10τ specimens in room air on 2.3 mm thick, 25.4 mm wide, C(T) specimens which satisfy the plane strain and small scale yielding requirements from ASTM standard E399 [39]. Prior to annealing, all samples were polished to a 0.05 μm surface finish on both faces and fatigue pre-cracked. Fatigue cycling was done using a computer-controlled, servo-hydraulic mechanical testing machine with a frequency, ν, of 25 Hz (sine wave) and a constant load ratio (ratio of minimum to maximum load, $R = P_{min}/P_{max}$) of 0.1. Fatigue crack growth rates, da/dN, were measured as a function of the applied stress intensity range, $\Delta K = K_{max} - K_{min}$, in general accordance with ASTM standard E647 [40], where K_{max} and K_{min} are the maximum and minimum stress intensity experienced during the loading cycle. To measure the fatigue thresholds, ΔK_{TH}, samples were cycled in stress intensity control with a decreasing stress-intensity range (K-gradient, $d\Delta K/da/\Delta K = -0.08\ mm^{-1}$) until the measured growth rates approached $\sim 10^{-10}$ m cycle^{-1}. Higher crack growth rates were measured using a constant stress range, $\Delta\sigma$. Crack lengths were continuously monitored using unloading elastic compliance measurements from a 120 Ω strain gauge attached to the back face of the specimen, with crack lengths computed using the appropriate calibrations for the C(T) specimen [41].

Following growth-rate measurements, plane strain fracture toughness values were determined by monotonically loading the fatigue precracked specimens to failure with a displacement rate of 20 μm s^{-1} in general accordance with ASTM standard E399. After fracture and fatigue experiments, the fracture surfaces of the specimens were analyzed using scanning electron microscopy (SEM).

3.3. Stress-life and fatigue crack initiation experiments

Fatigue life (S–N) curves were measured for both the SR and 10τ samples by cycling $2.3 \times 2.0 \times 85.0$ mm rectangular beams in four-point bending with an inner span, S_1, and outer span, S_2, of 30 mm and 60 mm, respectively, using a computer-controlled electromagnetic testing machine. The corners of the beams were slightly rounded to reduce stress concentration along the beam edges and they were polished to a 0.05 μm finish on the tensile surface prior to annealing. Testing was conducted in room air under load control using a sinusoidal waveform and a load ratio of $R = 0.3$. Compared to the fatigue crack growth rate measurements, a higher load ratio was used for these experiments to keep the specimens from vibrating out of the fixture.

Once cyclic loading began, testing was interrupted at regular intervals and specimens were inspected using optical microscopy (OM) in order to record the initiation of surface cracks during the fatigue test. If no damage was observed, the number of cycles between intervals was increased. Accordingly, a test frequency of 5 Hz was employed early in these experiments to allow frequent observations, while 20 Hz was used to generate adequate cycles as the inspection interval increased above $\sim 10^3$ cycles. Cellulose acetate tape replication was also used as a complimentary inspection and record-keeping method [42]. Acetate tape was softened with acetone and held against the tensile surface of the specimen until the acetone evaporated and the tape hardened. Features on the specimen surfaces were reproduced on the acetate negatives and allowed records of the crack initiation to be kept in case the initial inspections failed to observe the first fatigue cracks.

After the fatigue life experiments were concluded, the replicas and fracture surfaces were examined using OM and SEM. Replicas were coated with a thin layer of gold prior to SEM examination.

3.4. Depth-profiled position annihilation spectroscopy (PAS)

Spatial variations in free volume associated with fatigue deformation during crack growth experiments were assessed using depth-profiling, beam-based PAS, specifically utilizing the Doppler-broadening spectroscopy (DBS) technique. Full details are reported elsewhere [43], with a brief synopsis given here. Depth-profile measurements of the S parameter were made on the fatigue fracture surfaces of the as-cast, 10τ and SR C(T) specimens in a location where ΔK was $\sim 1.5\ MPa\sqrt{m}$, i.e., near the fatigue threshold. Positrons emitted from a radioactive Na^{22} source were confined and transported to the specimen surface. Six beam energies were used ranging between 1.1 and 8 keV corresponding to mean positron implantation depths of less than 10 nm to 190 nm. Such depth-profiled results were compared to similar depth-profiled results taken on a polished face of the same specimen.

As the positrons annihilate with electrons in the material, two gamma rays with energies of precisely 511 keV are produced; however, the measured energy of annihilation may be Doppler-shifted due to any center of mass motion of the annihilating pair. The S parameter is defined as the fraction of all 511 keV events within a specified central region ±0.88 keV from the peak, which corresponds to annihilation at rest, or with valence electrons, to all of the 511 keV events [44]. Annihilation in open volume defects result in less high-momentum annihilation and lead to a higher S parameter, making DBS sensitive to changes in free volume in amorphous materials.

4. Results

4.1. Enthalpy recovery and free volume quantification

As shown in Fig. 1, samples annealed at 610 K show a large endothermic heat recovery in the glass transition region, whereas the "unrelaxed" as-received and stress-relieved (SR) samples do not exhibit this effect. Enthalpy recovery increases with increasing annealing time. The amount of enthalpy, ΔH, that was released during the

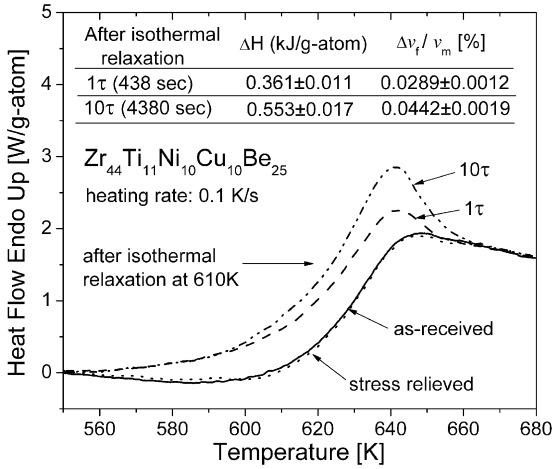

Fig. 1. Enthalpy recovery measurements in the glass transition region after isothermal relaxation at 610 K for 1τ and 10τ. In addition, the measurements for the unrelaxed samples in their as-received and stress-relieved states are shown. Corresponding enthalpy recovery measurements and quantification of free volume relaxation are reported in the table (inset).

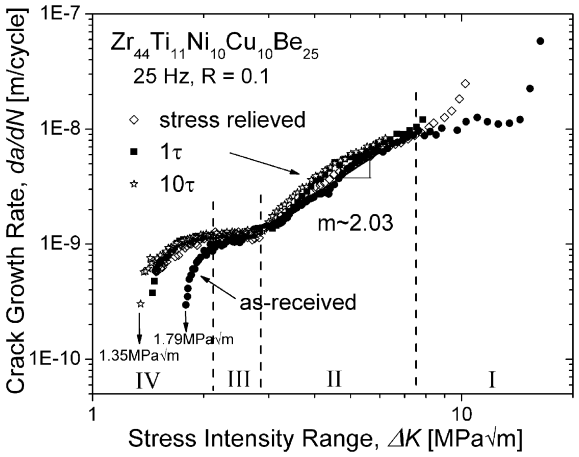

Fig. 2. Fatigue crack growth rates, da/dN, plotted as a function of the applied stress intensity range, ΔK, for different free volume and/or residual stresses states of $Zr_{44}Ti_{11}Ni_{10}Cu_{10}Be_{25}$. The four distinct growth rate regimes are annotated.

isothermal heat treatment, and recovered during reheating the sample, was determined within $\pm 3\%$[3] from the area between the curve of the relaxed sample and the unrelaxed sample (Fig. 1). The measured enthalpy recoveries, ΔH, for the 1τ and 10τ samples were reported in Ref. [35] and are given in the inset of Fig. 1. Furthermore, Fig. 1 shows that the SR sample annealed at 573 K for 2 min does not show any enthalpy recovery in the glass transition region relative to the as-received material; they are indeed in the same enthalpy state, and by extension in the same free volume state.

Assuming ΔH is proportional to the variation of the average free volume per atom, v_f/v_m, [30]:

$$v_f/v_m = \beta \cdot \Delta H, \tag{3}$$

where β was determined to be 0.080 ± 0.001 (kJ g^{-1} atom^{-1})$^{-1}$ for $Zr_{44}Ti_{11}Ni_{10}Cu_{10}Be_{25}$ [35], ΔH is given in kJ g^{-1} atom^{-1}, and v_f/v_m is in %. The atomic volume, v_m, of Vitreloy 1 has been reported as 1.67×10^{-29} m^3 near the liquidus [45]. Therefore, based on Eq. (3) and enthalpy recovery measurements, the reduction of free volume difference via structural relaxation, $\Delta v_f/v_m$, was determined. Results are provided in the inset of Fig. 1. Previous high-resolution transmission electron microscopy (HRTEM) studies have demonstrated that no nanocrystalization occurs in the 10τ annealed samples [35].

4.2. Fatigue crack growth behavior

The effect of free volume and stress relaxation on fatigue crack growth behavior is shown in Fig. 2, where growth rates, da/dN, are plotted as a function of the applied stress intensity range, ΔK. Four distinct growth rate regimes were observed: (I) a high-growth-rate regime corresponding to final fracture when the applied K_{max} reaches the fracture toughness of the material, (II) a mid-growth-rate regime in which the crack growth increases with the applied ΔK, (III) a near-threshold region with the crack growth rate relatively insensitive to the applied K and, (IV) a distinct threshold region with high sensitivity of the growth rate to the applied ΔK.

The mid-growth rates (regime II) were fitted to a Paris power law relationship [46]:

$$\frac{da}{dN} = C\Delta K^m \tag{4}$$

Using units of m cycle^{-1} and MPa$\sqrt{}$m in Eq. (4), C and m were found to be similar for all four cases with mean values and standard deviations of $(1.8 \pm 0.2) \times 10^{-10}$ and 2.03 ± 0.08, respectively. Measured fatigue crack growth thresholds, ΔK_{TH}, were in the range of 1.35–1.79 MPa$\sqrt{}$m, typical of Zr-based bulk metallic glasses [3,4,17,47–50]. Surprisingly, free volume relaxation does not influence the fatigue crack growth rates, da/dN, and fatigue thresholds, ΔK_{TH}. Conversely, residual stresses in the as-received material do affect the fatigue crack growth behavior, specifically by shifting ΔK_{TH} and the fracture toughness to higher values.

4.3. Fracture toughness behavior

Plane strain fracture toughness, K_{IC}, experiments showed that annealing has a degrading effect on the fracture toughness, as shown in Fig. 3. Removal of residual stresses at constant free volume decreased K_{IC} by ~33% from 51 MPa$\sqrt{}$m to 34 MPa$\sqrt{}$m. Relaxation for 1τ shows a minimal degrading effect on the fracture toughness with $K_{IC} = 32$ MPa$\sqrt{}$m. However, after relaxation for 10τ, the toughness shows a dramatic reduction in K_{IC} to 3 MPa$\sqrt{}$m,

[3] The 3% error on the enthalpy recovery measurements was calculated based on the sensitivity of the DSC, 0.2 μW, and the accuracy of the integration.

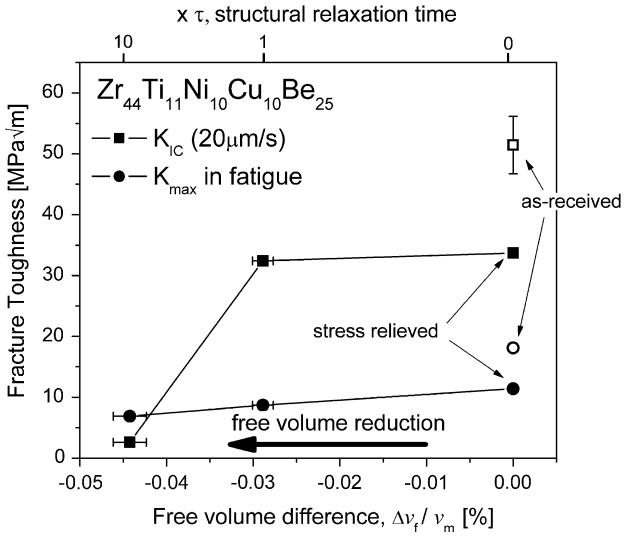

Fig. 3. Plain strain fracture toughness, K_{IC}, and instability fracture in fatigue crack propagation tests, K_{max}, for the as-received and annealed samples. Annealing to relieve residual stresses or reduce the free volume generally degrades the toughness. The error bars on $\Delta v_f/v_m$ indicate error estimates in the calculations, while the error bars on K_{IC} for the as-received specimens corresponds to the standard deviation of three K_{IC} tests.

an order of magnitude drop as compared with the stress-relieved material.

In fatigue, the effects of free volume reduction and residual stresses on the K_{max} values at the point of unstable fracture are similar to the effects on K_{IC}. Residual stress removal lowered K_{max} by ~39% from 18 MPa$\sqrt{m}$ to 11 MPa$\sqrt{m}$, and the degrading effect of free volume reduction on the toughness is still clearly observed. However, the toughness degradation at 10 τ is not as dramatic, with K_{max} at fatigue fracture falling to 7 MPa$\sqrt{m}$.

In most cases, K_{max} values at the point of unstable fracture in fatigue were lower than the K_{IC} values, consistent with previous studies that measured lower toughness with higher loading rate in metallic glasses [4]. However, fatigue cycling actually increased the fracture toughness of the 10τ relaxed specimen from 3 to 7 MPa$\sqrt{m}$ (Fig. 3).

4.4. Stress-life (S–N) behavior and crack initiation

The normalized stress amplitude, σ_a/σ_u, is plotted as a function of cycles to failure, N_f, in Fig. 4, where the stress amplitude, σ_a, is ½($\sigma_{max} - \sigma_{min}$). Data is normalized by the ultimate tensile strength, σ_u, reported in the literature, 1900 MPa [51]. The effect of free volume reduction is investigated by comparing the stress-life data for the 10τ and SR specimens, both of which are free of residual stresses. The stress-life fatigue data show that a free volume reduction affects the fatigue life at a given value of σ_a/σ_u, with the curves crossing each other at ~10^4 cycles and $\sigma_a/\sigma_u \sim 0.17$. At lower stress amplitudes ($\sigma_a < 325$ MPa), fatigue lifetimes are significantly shorter for the material with more free volume, and vice versa at higher stress

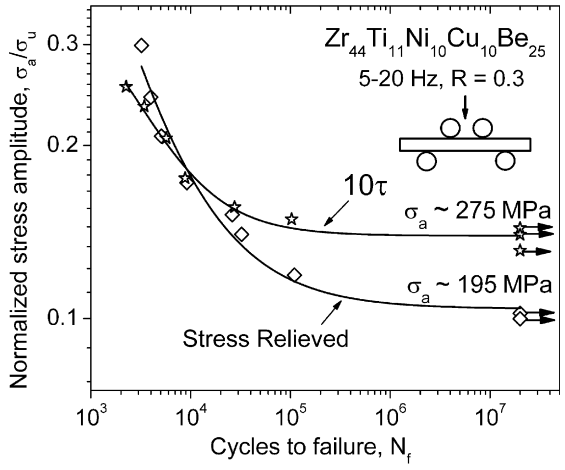

Fig. 4. Stress/life fatigue data for the 10τ and stress relieved specimens presented in terms of the normalized stress amplitude, σ_a/σ_u, plotted as function of cycles to failure, N_f.

amplitudes ($\sigma_a > 325$ MPa). Additionally, a reduction of free volume increases the fatigue strengths whereby the 10τ and SR specimens were found to display 2×10^7 cycle fatigue strengths at σ_a/σ_u values of 0.14 and 0.10, respectively. Those values are higher than previously reported for Zr–Ti–Cu–Ni–Be BMGs tested in four-point bending [3,52]. The improvement of the 2×10^7 cycle fatigue strength by free volume reduction is consistent with a previous study on $Zr_{41.25}Ti_{13.75}Ni_{10}Cu_{12.5}Be_{22.5}$ [9].

Examination of tensile surfaces and replicas indicated that damage initiation represents the majority of high-cycle fatigue life in both cases, as indicated in Fig. 5, which shows the number of cycles to crack initiation, N_i, for the various stress amplitudes tested. In Fig. 5, the error bars represent the cycle interval in which initiation was recorded. N_i was found to be affected by free volume changes in a similar way to N_f (Fig. 4). For $\sigma_a/\sigma_u < 0.17$,

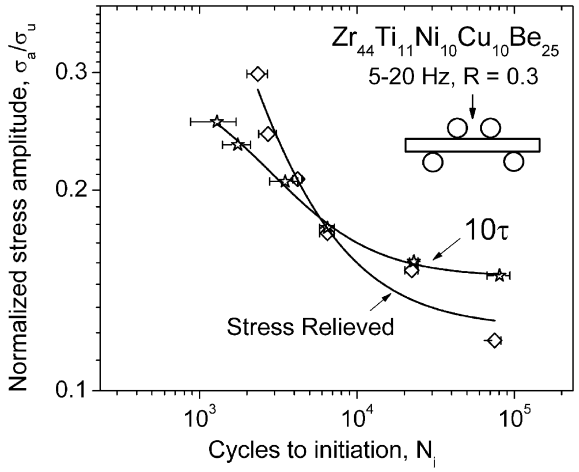

Fig. 5. Normalized stress amplitude, σ_a/σ_u, plotted as function of number of cycles to crack initiation, N_i. The error bars represent the cycle interval in which initiation was recorded.

damage initiation is retarded by free volume reduction, and vice versa at higher stress amplitude (>0.17).

In both materials, the damage originated in multiple locations on the tensile surface and rounded corners of the beams. It was observed that surface cracks were as likely to cause failure as corner cracks and that damage preferentially initiated at surface defects such as fine polishing scratches. Cracks were observed to initiate as shear bands or mixed-mode cracks that initially propagated at ~49° to the maximum normal stress axis (Fig. 6) similar to that observed in Ref. [52]. As observed previously [52], the cracks abruptly change growth direction and continue to propagate perpendicular to the tensile axis (Fig. 6) as mode I cracks until failure. It is thought that the change in direction occurs to maximize the mode I stress intensity, ΔK_I, once the shear band or mixed-mode crack has a mode I loading component above the mode I fatigue threshold, ΔK_{TH} [52].

Once one or more cracks initiated, the 10τ and SR specimens required the same number of cycles to failure at a given stress amplitude. This is demonstrated in Fig. 7, where the number of cycles to failure after initiation, $N_f - N_i$, for the SR samples is plotted as a function of cycles to failure after initiation for 10τ samples. A first-order linear fit, i.e. $y = x$, of the data shows that $(N_f - N_i)_{10\tau} \approx (N_f - N_i)_{SR}$. Such results indicate that the free volume reduction does not affect the growth rates and are in full agreement with the fatigue crack growth results in Fig. 2.

4.5. Fractography

Fatigue fracture surfaces of the different specimens had identical morphologies at a given growth rate. In near-threshold regions, the surface exhibits a featureless mirror-like appearance with the fatigue surfaces becoming rougher with increasing ΔK (Fig. 8). Examination of the bend beam fracture surfaces revealed that the cracks grew in a semi-elliptical shape (Fig. 9a). In general, fatigue striations were visible over regions of the crack surface for growth rates above $\sim 10^{-9}$ m cycle^{-1} for all the specimens, consistent with a previous report [49]. Such striations can be seen in Fig. 9b. Finally, overload fracture surfaces exhibited a vein-like morphology (Fig. 9b) typical of metallic glasses [53].

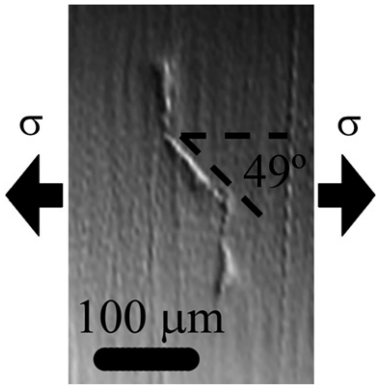

Fig. 6. Optical microscope image of tensile surface of an SR bend beam showing fatigue damage typically observed in both the 10τ and SR fatigue life tests. This particular image was taken after 2500 cycles at $\sigma_a = 568$ MPa.

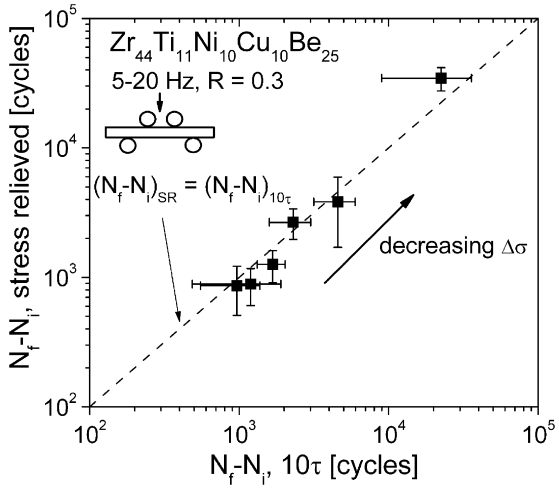

Fig. 7. Number of cycles to failure after initiation, $N_f - N_i$, for SR samples is plotted as a function of cycles to failure after initiation for 10τ samples. A first-order linear fit, i.e., $y = x$, of the data indicates that $(N_f - N_i)_{10\tau} \approx (N_f - N_i)_{SR}$ with $R^2 = 0.9926$.

4.6. Depth-profiled Doppler-broadening spectroscopy (DBS)

The bulk S parameter for the as-cast, 10τ and SR samples was found to be ~0.523. Recent positron annihilation lifetime spectroscopy (PALS) and DBS results suggest that the size distribution of the free volume elements is bi- or tri-modal prior to deformation [26,28,29,54,55]. For this BMG, the fact that DBS is not sensitive to the free volume changes from structural relaxation suggests that every positron is finding a free volume element to trap in, and free volume changes due to structural relaxation do not significantly change the size of the trapping free volume elements. This is consistent with the concept that the quantity, and not the size, of the various free volume defects changes with structural relaxation [56].

Depth-profiled DBS results from the fatigue fracture surface of a 10τ sample are given in Fig. 10, which was typical for all three specimens. All three depth profiles of the fracture surfaces showed an increased S parameter within a 30–50 nm surface layer that asymptotically approaches the bulk S value of ~0.523 with increasing depth. Such results indicate that the intense deformation at the fatigue crack tip has a significant effect on the local free volume. The increase in S parameter suggests: (i) free volume is being created at the crack tip during fatigue crack propagation, and (ii) the new free volume involves a different (larger) type of defect than is found in the undeformed regions. A more complete description of the PAS findings for these samples has been reported elsewhere [43].

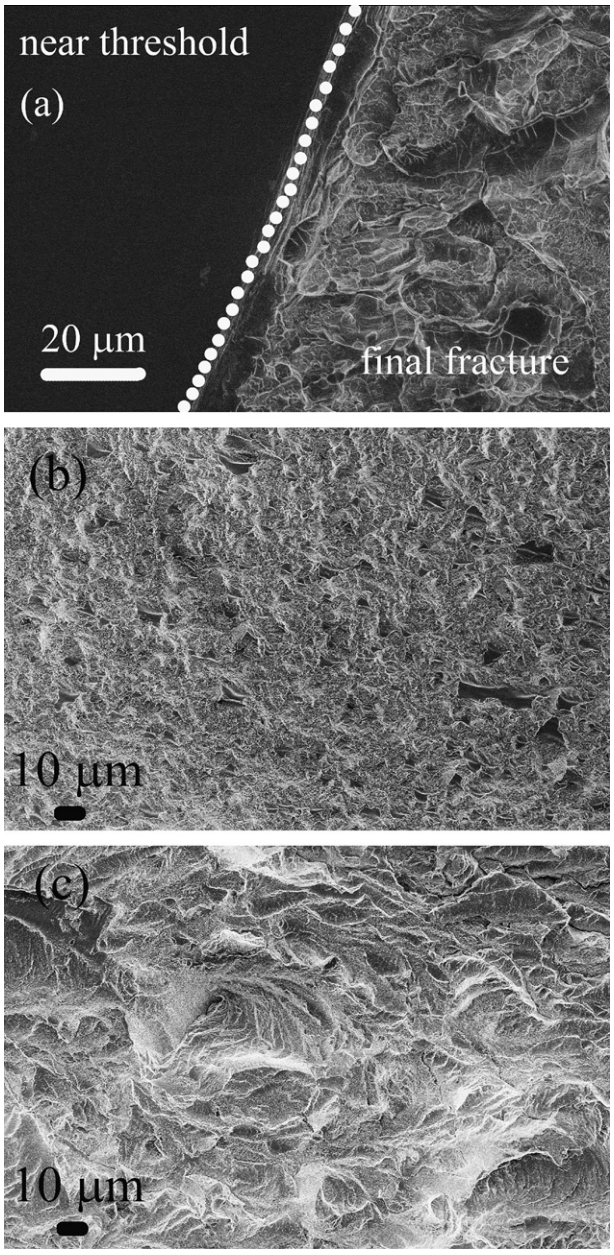

Fig. 8. Scanning electron micrographs of fracture surfaces showing: (a) the boundary between smooth near-threshold fatigue ($\Delta K \sim 1.8$ MPa$\sqrt{\text{m}}$ and $da/dN \sim 3 \times 10^{-10}$ m cycle^{-1}) and rough final fracture surface in an as-received specimen, (b) the fatigue crack growth region in a 10τ sample at mid level $\Delta K \approx 3$ MPa$\sqrt{\text{m}}$ and $da/dN \approx 10^{-9}$ m cycle^{-1}, and (c) the fatigue crack growth region in a 10τ sample at high level $\Delta K \approx 6$ MPa$\sqrt{\text{m}}$ and $da/dN \approx 10^{-8}$ m cycle^{-1}. All micrographs are of C(T) specimens and demonstrate the general trend of rougher surfaces with higher ΔK levels. Nominal crack growth direction was left to right.

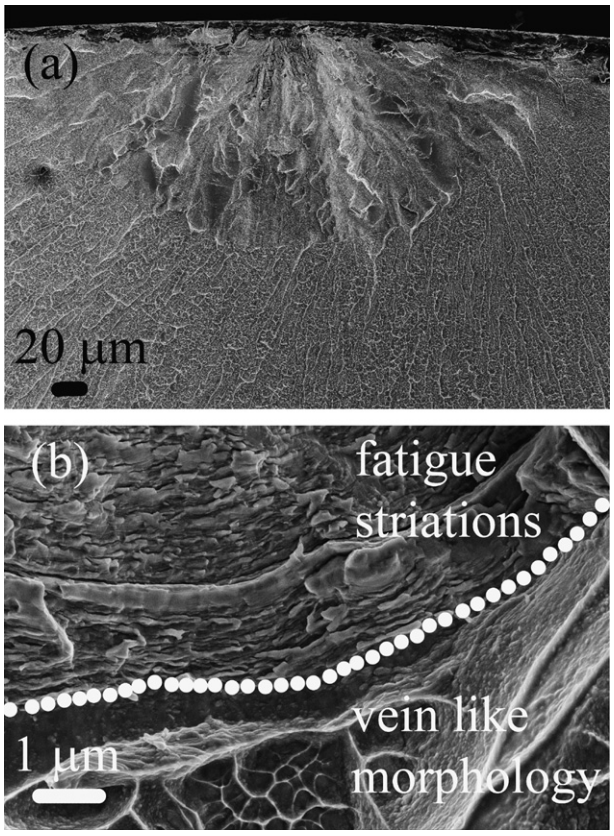

Fig. 9. Scanning electron micrographs of a stress-relieved bend-beam fracture surface showing: (a) semi-elliptical stable fatigue region, and (b) the transition between stable growth and unstable fracture. Nominal crack growth direction is top to bottom and $\sigma_a = 290$ MPa. In (b) note the fatigue striations observed at the top of the micrograph, and the vein-like overload fracture morphology in the bottom of the micrograph, both of which are typical of metallic glasses.

5. Discussion

5.1. Mechanisms of fatigue crack growth

It is apparent from Fig. 3 that a reduction in free volume by structural relaxation embrittles bulk metallic glasses. Existing models for the deformation of metallic glasses predict that a reduction in free volume will retard plastic

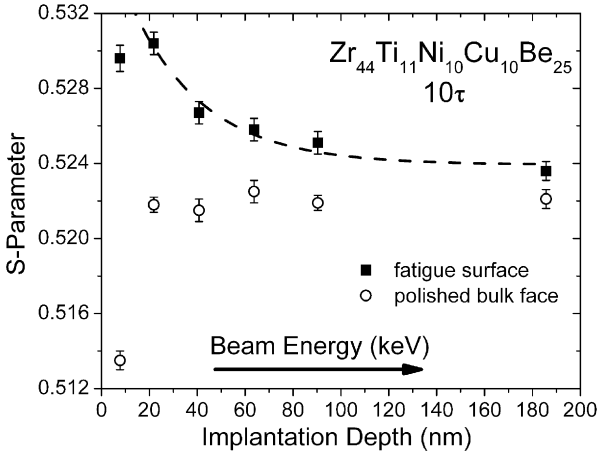

Fig. 10. Beam-based depth-profiled PAS Doppler-broadening results for the 10τ C(T) specimen taken from Ref. [43]. The fraction annihilating with valence electrons, S, is plotted as a function of the implantation depth. Depth-profiling was performed on the cyclically loaded (fatigue) surface where ΔK was ~1.5 MPa$\sqrt{\text{m}}$ and compared to measurements taken on the polished faces of each sample.

deformation [13–15] and it logically follows that the reduced ductility will result in less crack-tip blunting and lower fracture toughness (Fig. 3 and Refs. [9,17,18,20]). It is thus surprising that fatigue crack growth, which is believed to result from alternating crack blunting and resharpening [4], is not affected by change in the free volume (Fig. 2). Indeed, Suh et al. showed that when the free volume of Vitreloy 1 is filled with hydrogen, both the fracture toughness and the fatigue crack growth properties are affected [17,18]. Thus, the mechanism for fatigue crack growth in BMGs must account for all of these observations.

During inhomogeneous plastic flow in BMGs, the deformation is highly localized in shear bands and it has been reasoned that the observed softening in those shear bands must be due to local free volume generation within the bands [13–15]. Additionally, molecular-dynamics simulations of deformation in binary metallic glasses, both three-dimensional with 8000 atoms [57] and two-dimensional with 20,000 atoms [58], show softening and shear localization that is associated with free volume production. Also, recently high-resolution TEM imaging techniques [59–62] and positron annihilation spectroscopy [26,29] have revealed that regions of localized plastic deformation (shear bands) in bulk metallic glasses contain a high concentration of thermodynamically stable sub-nanometer scale voids. These voids apparently result from the coalescence of excess free volume upon cessation of the flow.

Thus, based on the current understanding of flow in metallic glasses, it is expected that the large plastic strains near a crack tip will be associated with a local increase in free volume. The DBS results presented in Fig. 10 confirm that this is the case; indeed, the free volume is locally higher where the fatigue crack propagated. As the crack propagates it is enveloped with a fatigue transformation zone, as illustrated in Fig. 11. Free volume is generated within this zone, with the amount expected to decrease with increasing distance from the crack flanks or tip. A first-order estimate for the total extent of the transformation zone on the fatigue surface would be the mode I plastic zone radius, r, for plane strain and along the axis perpendicular to the crack plane as given by:

$$r \approx \frac{1}{2\pi}\left(\frac{K_I}{\sigma_Y}\right)^2, \tag{5}$$

where K_I and σ_Y are the maximum stress intensity and yield strength, respectively. Near the fatigue threshold ($K_I \approx 1.67$ MPa$\sqrt{\text{m}}$), r is predicted to be ~122 nm. Furthermore, a significantly higher increase in free volume would be expected within the cyclic plastic zone where reversed plastic flow occurs during each cycle, which is generally ~1/4 the total plastic zone size [63,64], or ~31 nm. The direct applicability of Eq. (5) to the inhomogeneous flow in BMGs is uncertain; however, depth-profiled DBS detected a definite increase in S within a 30–50 nm layer,

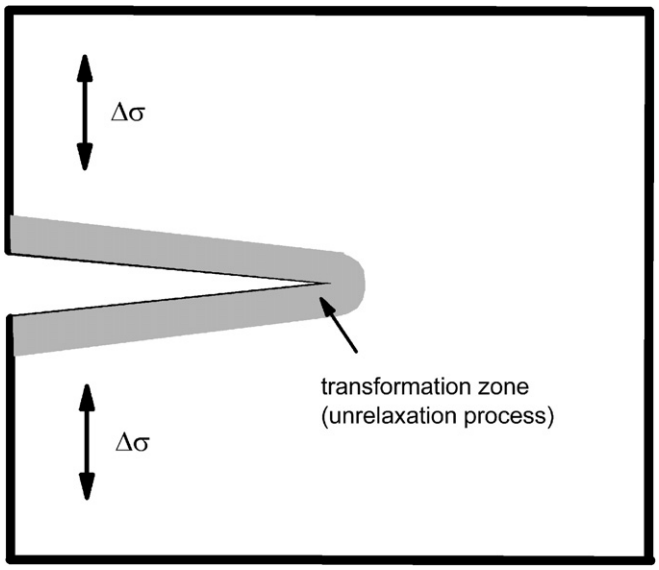

Fig. 11. Schematic of a fatigue transformation zone in a BMG. The stress/strain concentration at the crack tip induces an increase in free volume and as the crack propagates it is enveloped with a transformed zone.

which is consistent with an increase in free volume within the cyclic plastic zone.

The transformation zone discussed is similar to the martensitic transformation zones that occur in partially stabilized zirconia [65,66] or austenitic stainless steel [67,68], although in those cases the volume increase is due to a phase transformation from one crystal structure to another. In those cases, the large volume expansion (2–4%) associated with the martensitic transformation generates a residual stress field that puts the crack under compression, reducing crack propagation rates. In bulk metallic glasses, the total volume increase is orders of magnitude smaller and is not large enough to cause significant compressive stresses on the crack tip based on models for transformation toughening [69,70]. Based on the weight function method developed by McMeeking and Evans [70], a 1 MPa$\sqrt{\text{m}}$ reduction in the maximum stress intensity at the crack tip near the threshold would require a total volume expansion of ~10% within a 100 nm thick transformation zone. Additionally, the average free volume per atom of the $Zr_{44}Ti_{11}Ni_{10}Cu_{10}Be_{25}$ bulk metallic glass can be estimated from Ref. [35], and was found to represent roughly 0.1% of the total volume when considering only the smallest atoms, beryllium, and the hard sphere model. Therefore, this means that the free volume would have to expand by two orders of magnitude in order to decrease the stress intensity by 1 MPa$\sqrt{\text{m}}$ near the fatigue threshold. Kanungo et al. [28,71] observed that cold-rolling to a thickness of 32% increased the free volume of $Zr_{58.5}Cu_{15.6}Ni_{12.8}Al_{10.3}Nb_{2.8}$ bulk metallic glass by 4.4% relative to the undeformed state. Even though the free volume was averaged over the entire specimen and is believed to be much larger within the shear band, it is apparent that the total volume increase by free volume expansion is largely

insufficient to generate a significant compressive residual stress field.

However, it appears that the newly created free volume in the fatigue transformation zone determines the local flow properties, making the fatigue crack growth behavior relatively insensitive to bulk free volume differences. Accordingly, a new mechanism for fatigue crack growth in bulk metallic glasses is proposed, where crack advance involves the creation of a fatigue transformation zone with flow properties independent of the bulk material, and alternating crack blunting and resharpening occurs within this zone. Such a mechanism is consistent with the hydrogen charging results of Suh et al. [17,18], which showed a pronounced affect on the crack growth rates when the bulk free volume was filled with hydrogen. In that case, the extra free volume created in the fatigue transformation zone would be quickly filled with the highly mobile hydrogen, effecting the crack growth rates. However, this new mechanism implies that simply changing the bulk free volume of a BMG will not necessarily affect the fatigue crack growth behavior, as seen in Figs. 2 and 7.

There are still unresolved questions regarding the fatigue crack growth mechanism in BMGs; however, noting that there is an unexplained region of the fatigue crack growth curve that is largely independent of the applied ΔK, i.e., where $da/dN \approx 10^{-9}$ m cycle^{-1} (Fig. 2, regime III). Such behavior is common when there is an environmental effect on crack growth and the crack growth rate is limited by diffusion of an environmental species to the crack tip [72], although it is currently unclear if that is the case with Zr-based BMGs.

5.2. Toughening mechanisms

As observed in Fig. 3, the degrading effect of structural relaxation on the fracture toughness is significantly weaker under cyclic loading (K_{max}) as opposed to monotonic loading (K_{IC}). Furthermore, fatigue cycling appears to increase the fracture toughness of the 10τ relaxed specimen. It is important to note that the fracture toughness of metallic glasses is a strain-rate-sensitive property, and higher strain rates, as experienced during unstable fracture at the end of a constant stress fatigue test, generally have been shown to give lower fracture toughness [4].

The higher fracture toughness for the 10τ specimen measured during fatigue testing is not surprising, however, when one considers the concept of a fatigue transformation zone. All K_{IC} measurements were done using fatigue precracked specimens where the final ΔK value experienced before the fracture toughness test was near the fatigue threshold. Accordingly, the fatigue transformation zone would be small in those cases, and much smaller than the plastic zone created during the fracture test, i.e., by a factor of 5 for 10τ specimen, and by two orders of magnitude for the SR specimen, based on Eq. (4). Thus, for the K_{IC} tests, the existence of a fatigue transformation zone would be expected to have a small or negligible effect.

Unstable fracture at the end of a constant stress fatigue test is a very different situation. In that case, the ΔK value for the cycle just before instable fracture is high, and the fatigue transformation zone is relatively large compared to the K_{IC} test. Accordingly, for this case there will be two partially offsetting effects whereby the high strain rate is lowering the toughness, while the extra free volume in the large fatigue transformation zone enhances the toughness. The relative magnitude of these two effects will determine how the fracture toughnesses measured at the instability of the fatigue test compares to conventionally measured K_{IC} values. For the 10τ sample, the effect of the fatigue transformation zone is beneficial enough to give a higher fracture toughness value in fatigue relative to the quasi-static K_{IC}. Thus, the fatigue transformation zone can be thought of as an intrinsic toughening mechanism, whereby the local ductility at the crack tip is enhanced.

5.3. Fatigue life

Figs. 2 and 7 show that free volume relaxation does not have an influence on fatigue crack growth rates, da/dN, and fatigue thresholds, ΔK_{th}. However, a reduction of free volume improves the fatigue limits and affects the fatigue lifetimes (Fig. 4 and in Ref. [9]). Based on Fig. 5, it is clear that the effect on the fatigue life data is due to effects on the crack initiation portion of the fatigue lifetime. Mechanistically, this may be understood by considering that fatigue cracks tend to initiate from slip bands (Fig. 6). The larger amount of free volume in the SR material allows easier deformation and easier formation of slip bands, leading to faster crack initiation possibly caused by nanovoids [59–62] or nanocrystals [73] that form within the shear bands that act as damage initiation sites.

In the absence of residual stresses, $Zr_{44}Ti_{11}Ni_{10}Cu_{10}Be_{25}$ spends most of its fatigue life in crack initiation, as shown in Figs. 5 and 7. Note that this is in contrast with a study on a similar Zr-based alloy composition which reported that fatigue crack initiation occurs within the first few cycles [52]. It is currently unclear why these materials behaved very differently, but possibilities include: (i) fundamental differences between the alloys, and/or (ii) other factors such as residual stresses, defects, or other inhomogeneities. Indeed, bending beams were not stress-relieved in Ref. [52], and depending on the orientation and machining of the beams, the tensile surface during the bending tests may have had residual tensile stresses which contributed to early crack initiation. Additionally, defects or inhomogeneities in the BMG could also have accounted for much quicker crack initiation.

5.4. Role of residual stresses

As mentioned earlier, bulk metallic glasses develop residual stresses during processing due to thermal tempering. It has been shown in previous studies [11,12] that compressive stresses on the order of several hundred MPa can

occur on the surface of as-cast metallic glasses, with offsetting tensile stresses below the surface. The effects of residual stresses have often been ignored in the published literature on mechanical properties; however, the present results illustrate how residual stresses are of primary importance in determining the fracture and fatigue properties (Figs. 2 and 3). Specifically, residual compressive stresses on the specimen surfaces reduce the crack propagation rate in the threshold region and improve the fracture toughness. In the present study these increases were significant, 33% and 50% increases for ΔK_{TH} and K_{IC}, respectively. Furthermore, although not explicitly measured in this study, those combined effects are expected to have a significant effect on the overall fatigue lifetime.

The mechanism responsible for these effects is presumed to be that the compressive thermal tempering stresses superimpose onto the crack tip stress field, and therefore lower the stress intensity at the crack tip. Although that mechanism only acts on the specimen surfaces where the residual stresses are compressive, it is clearly significant enough to affect the overall properties (Figs. 2 and 3).

The effect of residual stresses likely explains some of the scatter observed in published fracture and fatigue data, such as the large scatter in ΔK_{TH} seen in Ref. [3]. Thus, when testing BMGs without first relieving the residual stresses, it is important that those residual stresses be characterized and reported along with the data. Several methods have been developed for characterizing residual stresses in BMGs, including a crack compliance method [11,12] and high energy X-ray scattering [74].

5.5. Tailoring the fracture and fatigue properties of BMGs

Based on the results of the present study, it is clear that the fracture and fatigue properties of bulk metallic glasses are not solely determined by the chemical composition and can be tailored for a given application by adjusting the free volume and residual stresses. By reducing the free volume, one can enhance the fatigue life while sacrificing fracture toughness. However, both fracture and fatigue behavior can be enhanced by controlling the residual stresses, for example with post-processing treatments such as shot-peening [75]. Thus, careful control of free volume and compressive residual stresses can potentially be used to improve the overall properties of bulk metallic glasses and obtain desired characteristics, as shown schematically in Fig. 12.

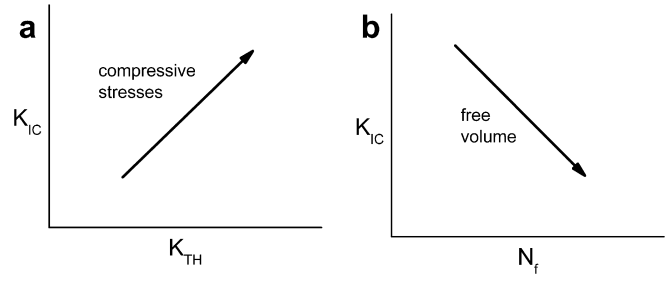

Fig. 12. Schematic illustrating how overall alteration of the fatigue and fracture properties in BMGs can be obtained by concurrently controlling: (a) residual stresses to improve both the fatigue threshold, K_{TH}, and the fracture toughness, K_{IC}; and (b) the free volume to improve the fatigue limit but degrade the fracture toughness, K_{IC}.

6. Conclusions

Based on a study of the fracture and fatigue behavior of a $Zr_{44}Ti_{11}Ni_{10}Cu_{10}Be_{25}$ bulk metallic glass, with specific attention paid to the effects of free volume variations and residual stresses, the following conclusions are made:

1. Both plane strain (K_{IC}) and fatigue (K_{max}) fracture toughness were found to be significantly degraded by a reduction in free volume via structural relaxation.
2. The fatigue crack growth rates were insensitive to free volume variations. Depth-profiled Doppler-broadening spectroscopy demonstrated that the large plastic strains near the fatigue crack tip cause a local increase in free volume. As the crack propagates, it is enveloped in a fatigue transformation zone that controls the local flow properties and makes the fatigue crack growth behavior insensitive to the initial free volume state.
3. A reduction of free volume improves the 10^7 cycle fatigue strength and affects the fatigue lifetimes specifically by increasing the number of cycles to cause crack initiation below $\sigma_a/\sigma_u \sim 0.17$.
4. Residual compressive stresses significantly affect the fatigue and fracture properties. Specifically, compressive thermal tempering stresses on the surface improve the fatigue threshold and fracture toughness by lowering the stress intensity at the crack tip by superposition of the residual stresses.
5. The overall fatigue and fracture properties can be tailored to desired properties by controlling the free volume and residual stresses.

Acknowledgements

This material is based on work supported by the National Science Foundation under Grant No. DMR-0205940. The authors gratefully acknowledge the help of Drs D.W. Gidley, R.S. Vallery and M. Liu at the University of Michigan Randall Physics Laboratory with the PAS measurements. The authors also thank Dr A. Peker of Liquidmetal© Technologies and Dr. J. Schroers from Yale University for supplying the material.

References

[1] Ashby MF, Greer AL. Scr Mater 2006;54:321.
[2] Schroers J. JOM 2005;57:35.
[3] Gilbert CJ, Lippmann JM, Ritchie RO. Scr Mater 1998;38:537.
[4] Gilbert CJ, Schroeder V, Ritchie RO. Metall Mater Trans 1999;30A:1739.
[5] Peter WH, Buchanan RA, Liu CT, Liaw PK. J Non-cryst Solids 2003;317:187.

[6] Peter WH, Liaw PK, Buchanan RA, Liu CT, Brooks CR, Horton Jr JA, et al. Intermetallics 2002;10:1125.
[7] Wang GY, Liaw PK, Peker A, Yang B, Benson ML, Yuan W, et al. Intermetallics 2005;13:429.
[8] Wang GY, Liaw PK, Peter WH, Yang B, Yokoyama Y, Benson ML, et al. Intermetallics 2004;12:885.
[9] Launey ME, Busch R, Kruzic JJ. Scr Mater 2006;54:483.
[10] Menzel BC, Dauskardt RH. Scr Mater 2006;55:601.
[11] Aydiner CC, Ustundag E. Mech Mater 2005;37:201.
[12] Aydiner CC, Ustundag E, Prime MB, Peker A. J Non-cryst Solids 2003;316:82.
[13] Spaepen F. Acta Metall 1977;25:407.
[14] Argon AS. Acta Metall 1979;27:47.
[15] Steif PS, Spaepen F, Hutchinson JW. Acta Metall 1982;30:447.
[16] Gerling R, Schimansky FP, Wagner R. Acta Metall 1988;36:575.
[17] Suh D, Dauskardt RH. Scr Mater 2000;42:233.
[18] Suh D, Dauskardt RH. Mater Sci Eng 2001;A319–321:480.
[19] Suh D, Dauskardt RH. J Non-cryst Solids 2003;317:181.
[20] Murali P, Ramamurty U. Acta Mater 2005;53:1467.
[21] Rehmet A, Gunther-Schade K, Ratzke K, Geyer U, Faupel F. Phys Stat Sol A 2004;201:467.
[22] Busch R, Johnson WL. Appl Phys Lett 1998;72:2695.
[23] Samwer K, Busch R, Johnson WL. Phys Rev Lett 1999;82:580.
[24] Spaepen F, Taub AI. Amorphous metallic alloys. Butterworth; 1983.
[25] Wu TW, Spaepen F. Phil Mag B 1990;61:739.
[26] Flores KM, Kanungo BP, Glade SC, Asoka-Kumar P. J Non-cryst Solids 2007;353:1201.
[27] Flores KM, Suh D, Dauskardt RH, Asoka-Kumar P, Sterne PA, Howell RH. J Mater Res 2002;17:1153.
[28] Kanungo BP, Glade SC, Asoka-Kumar P, Flores KM. Intermetallics 2004;12:1073.
[29] Flores KM, Sherer E, Bharathula A, Chen H, Jean YC. Acta Mater 2007;55:3403.
[30] van den Beukel A, Sietsma J. Acta Metall Mater 1990;38:383.
[31] Tuinstra P, Duine PA, Sietsma J, van den Beukel A. Acta Metall Mater 1995;43:2815.
[32] Daniel BSS, Reger-Leonhard A, Heilmaier M, Eckert J, Schultz L. Mech Time-Dependent Mater 2002;6:193.
[33] Hammond VH, Houtz MD, O'Reilly JM. J Non-cryst Solids 2003;325:179.
[34] Slipenyuk A, Eckert J. Scr Mater 2004;50:39.
[35] Launey ME, Kruzic JJ, Li C, Busch R. Appl Phys Lett 2007;91:051913.
[36] Hays CC, Kim CP, Johnson WL. Appl Phys Lett 1999;75:1089.
[37] Waniuk T, Schroers J, Johnson WL. Phys Rev B 2003;67.
[38] Shadowspeaker L, Busch R. Appl Phys Lett 2004;85:2508.
[39] ASTM E399-90 (Reapproved 1997). Annual Book of ASTM Standards, vol. 03.01: Metals – mechanical testing; elevated and low-temperature tests; metallography ASTM International, West Conshohocken, PA, 2004.
[40] ASTM E647-00. Annual Book of ASTM Standards, vol. 03.01: Metals – mechanical testing; elevated and low-temperature tests; metallography ASTM International, West Conshohocken, Pennsylvania, USA, 2004.
[41] Maxwell DC. Report AFWAL-TR-87-4046. Air Force Wright Aeronautical Laboratories; 1987.
[42] Swain MH. Monitering small-crack growth by the replication method. In: Larsen JM, Allison JE, editors. Small-crack test methods, ASTM STP 1149. American Society for Testing and Materials; 1992. p. 34.
[43] Vallery RS, Liu M, Gidley DW, Launey ME, Kruzic J. J Appl Phys Lett 2007. in review.
[44] Gidley DW, Peng H-G, Vallery RS. Annu Rev Mater Sci 2006;36:49.
[45] Ohsaka K, Chung SK, Rhim WK, Peker A, Scruggs D, Johnson WL. Appl Phys Lett 1997;70:726.
[46] Paris PC, Gomez MP, Anderson WP. Trend Eng 1961;13:9.
[47] Gilbert CJ, Ritchie RO, Johnson WL. Appl Phys Lett 1997;71:476.
[48] Flores KM, Johnson WL, Dauskardt RH. Scr Mater 2003;49:1181.
[49] Hess PA, Dauskardt RH. Acta Mater 2004;52:3525.
[50] Zhang ZF, Eckert J, Schultz L. Metal Mater Trans A 2004;35A:3489.
[51] Bruck HA, Christman T, Rosakis AJ, Johnson WL. Scr Metall Mater 1994;30:429.
[52] Menzel BC, Dauskardt RH. Acta Mater 2006;54:935.
[53] Pampillo CA, Reimschuessel AC. J Mater Sci 1974;9:718.
[54] Suh D, Dauskardt RH, Asoka-Kumar P, Sterne PA, Howell RH. J Mater Res 2003;18:2021.
[55] Nagel C, Ratzke K, Schmidtke E, Faupel F. Phys Rev B 1999;60:9212.
[56] Sietsma J, Thijsse J. Phys Rev B 1995;52:3248.
[57] Albano F, Falk ML. J Chem Phys 2005;122.
[58] Shi YF, Falk ML. Phys Rev Lett 2005;95.
[59] Jiang WH, Atzmon M. Acta Mater 2003;51:4095.
[60] Jiang WH, Pinkerton FE, Atzmon M. Acta Mater 2005;53:3469.
[61] Li J, Spaepen F, Hufnagel TC. Phil Mag A 2002;82:2623.
[62] Li J, Wang ZL, Hufnagel TC. Phys Rev B 2002;65.
[63] McClung RC. Fatigue Fract Eng Mater Struct 1991;14:455.
[64] Rice JR. In: Fatigue crack propagation. ASTM STP 415. ASTM; 1967. p. 47.
[65] Dauskardt RH, Marshall DB, Ritchie RO. J Am Ceram Soc 1990;73:893.
[66] Dauskardt RH, Yu W, Ritchie RO. J Am Ceram Soc 1987;70:C248.
[67] Mei Z, Morris Jr JW. Metall Mater Trans 1990;21A:3137.
[68] Mei Z, Morris Jr JW. Eng Fract Mech 1991;39:569.
[69] Evans AG, Cannon RM. Acta Metall 1986;34:761.
[70] McMeeking RM, Evans AG. J Am Ceram Soc 1982;65:242.
[71] Kanungo BP, Lambert MJ, Flores KM, Flores KM. Amorphous and nanocrystalline metals. In: Busch R, Hufnagel TC, Eckert J, Inoue A, Johnson WL, Yavari AR, editors. Materials Research Society; 2004. p. 429.
[72] Anderson TL. Fracture mechanics: fundamentals and applications. Taylor and Francis Group; 2005.
[73] Chen H, Shiflet GJ, Poon SJ. Nature 1994;367:541.
[74] Hufnagel, TC. Personal communication; 2007.
[75] Zhang Y, Wang WH, Greer AL. Nature Mater 2006;5:857.